City Research Online

City, University of London Institutional Repository

This is the published version of the paper.

This version of the publication may differ from the final published version.

Rotational and blockage effects on a wind turbine model based on local blade forces

View the article online for updates and enhancements.

Rotational and blockage effects on a wind turbine model based on local blade forces

R. Soto-Valle[1], M. Gualtieri[2], S. Bartholomay[1], M. Manolesos[3], C.N. Nayeri[1], A. Bianchini[2] and C.O. Paschereit[1]

[1] ISTA, Technische Universität Berlin, Müller-Breslau-Str. 8, 10623 Berlin, Germany

[2] DIEF, Università degli Studi di Firenze, via di Santa Marta 3, 50139 Firenze, Italy

[3] SMCSE, City, University of London, Northampton Square, London EC1V 0HB, UK

E-mail: `rodrigo.soto@campus.tu-berlin.de`

Abstract. This paper describes the results of an extended experimental campaign, reporting surface pressure measurement over one of the blades of the Berlin Research Turbine (BeRT), placed in a closed-loop wind tunnel facility. BeRT is a three-bladed horizontal axis wind turbine with a $3m$ rotor diameter. The focus is, on the one side, on the three-dimensional effects experienced by the rotating blade, in comparison to 2D approaches by means of XFoil simulations and 2D blade section experiments. On the other side, the blockage effects are investigated between the wind turbine model, placed in the wind tunnel where a 40% blockage ratio is produced, and lifting line free vortex wake simulations, where wind tunnel walls are not considered. Additionally, CFD computations are added in the comparison, with simulations of the far-field and with the wind tunnel walls. The turbine model is studied at several operational conditions such as different blade pitch angles and turbine yaw misalignments. Results are presented in terms of local force components derived from the surface pressure measurements. It is shown that rotational augmentation is evident at the blade mid-span location despite the large blockage. Additionally, the blockage is noticed by means of an offset in both normal and tangential local forces conserving trends and features under axial inflow and yaw misalignments. It is found that the offset in forces can be counteracted by pitching the blades.

1. Introduction

Wind tunnel measurements are an important source of information about several aspects of a wind turbine in controlled conditions. Nonetheless, these kinds of measurement also present drawbacks such as blockage, similarity parameter mismatch [1] or scalability, to name a few.

One common measurement technique, used to assess wind turbine models in wind tunnels, is surface pressure measurements. The latter is done by placing pressure taps at different locations along the rotor blade, which are used to obtain local forces over the blades. Several studies have been published regarding pressure measurements on rotating blades in the last years. Some relevant investigations are briefly described as follows.

The Unsteady Aerodynamics Experiments (UAE) [2, 3] and MEXICO [4] projects published important databases under different operational conditions in wind tunnel facilities. These measurement campaigns have allowed the validation of several numerical modeling tools that can capture the aerodynamics effects [5–8]. The rotational augmentation is reported after comparison with two-dimensional approaches. A clear influence of the rotation is exhibited in both stall delay and aerodynamic performance with a lift coefficient increment up to $\Delta C_l = 0.5$ in the blade mid-span. In both cases, a large-scale wind tunnel i.e., low blockage ratio is exhibited.

Furthermore, there are several ongoing projects of wind turbine models placed in various wind tunnel facilities [9–13].

The project PAK 780, funded by the German Science Foundation (DFG), focused its effort on the study of the wind turbine load control under realistic turbulent inflow conditions [14–16]. Under this project, the Technische Universität Berlin developed a scaled wind turbine model, the Berlin Research Turbine (BeRT). BeRT is a research horizontal axis wind turbine with three modular exchangeable blades that produces a 40% ratio blockage in the wind tunnel facility. The effects of the latter have been investigated by Klein et al. [17–19], using the CFD code FLOWer. They computed several scenarios to study the performance of BeRT under the influence of the wind tunnel walls, the wind turbine tower, and the contraction of the wind tunnel. The main conclusions showed that the largest effect is produced by the walls of the tunnel, which can increase the thrust and power output by 25% and 50%, respectively. Moreover, Soto-Valle et al. [20] studied the blade tip vortices behavior under the effect of wind tunnel walls through stereo particle image velocimetry experiments and without wall constraint by means of lifting line-free vortex wake (LLFVW) [21] simulations. The findings showed a more downstream and inboard trajectory of the blade tip vortices in the experiments. Additionally, BeRT has been the testbed for passive and active flow control devices, applied directly on the blade. A detailed setup and results can be found regarding Gurney flaps [22], vortex generators [23] and Trailing Edge Flaps (TEFs) [24].

This paper aims to describe the differences between BeRT test rig and several datasets regarding the local forces, which are the result of the pressure contribution. Both 2D and 3D approaches are taken into account. First, the well-known rotational augmentation concept is revised considering information from XFoil and a 2D-wing with the purpose of confirming the rotational effects despite the resulting blockage. Secondly, the blockage effect is investigated by examining computational and numerical tools against wind tunnel measurements. This represents an important source of information to support future wind tunnel experiments of small wind turbine models and to understand the origin of possible differences between experiments and simulations.

The following section, Sect. 2, gives an overview of the experimental and numerical datasets to compare. Subsequently, the methodology and the performance indicators to compare are introduced in Sect. 3. Results are presented in Sect. 4, while the most important remarks are made in Sect. 5.

2. Experimental and simulation setups
This section provides a brief description of the test rigs and simulations considerations in both the 2D and 3D approaches that subsequently are compared.

2.1. 2D approaches
Two datasets are considered in the 2D framework. On one hand, XFoil simulations, based on the Clark-Y airfoil (BeRT-blade profile), are performed with fixed parameters, which can be found in Table 1. Transition on the airfoil was left free (i.e., with the e^N transition model), assuming an average wind tunnel condition ($Ncr = 9$). These parameters have been chosen after a sensitivity analysis to match with the wind tunnel and wind turbine characteristics under axial inflow conditions and the local flow features at the radial station at $45\%R$.

On the other hand, a 2D-wing experimental dataset based on the Clark-Y profile is added to the comparison. These experiments were originally presented in the work of Bartholomay et al. [25]. The wing has a chord-length of $c = 0.305\ m$ and a span-length of $s = 0.8\ m$. The wind tunnel inflow velocity was set to reach a $Re = 2.9 \times 10^5$ based on the chord-length and inflow speed. Additionally, the turbulence intensity of the freestream velocity was below 0.3% [26]. A total of 32 pressure taps, located chordwise on the 2D-wing surface, were measured. The wing

Table 1. Summary of the XFoil parameters.

parameter	value
panels	300
Re	2.9×10^5
Ncr	9
Ma	0
AoA range	$0° - 15°$
ΔAoA	$0.1°$

(see Fig. 1) is equipped with an actuated TEF. Due to the hinge between the main body and TEF, no pressure taps are located between the chord range $x/c = 0.5 - 0.8$. It is worth noticing that the results used in the present work only consider steady conditions i.e., both the wing TEF and the wind tunnel active grid are in their neutral position.
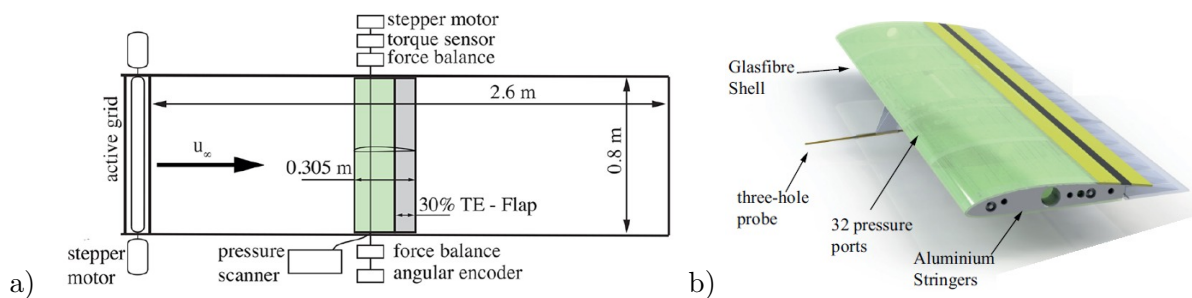
Figure 1. Details of the 2D experiment approach. a) Scheme of the wind tunnel setup. b) Sketch of the tested 2D-wing. Modified from Bartholomay et al. [25].

2.2. 3D approaches

The experiments are the result of an extended measurement campaign, where the model was placed in the closed-circuit wind tunnel at the Hermann-Föttinger Institut of the Technische Universität Berlin. BeRT is a three-bladed upwind horizontal axis wind turbine with a rotor radius of $R = 1.5\ m$.

The wind tunnel freestream velocity and the turbine rotational speed were set to run the turbine at the rated tip speed ratio of $TSR = 4.3$. Additionally, BeRT was tested under the following operational conditions:

(i) he blade pitch angle was swept between $\theta = -10°$ and $\theta = 10°$ with increments of $\Delta\theta = 2°$

(ii) Axial inflow condition, $\psi = 0°$

(iii) The turbine yaw angle was chosen for two misalignments, $\psi = -15°$ and $\psi = -30°$
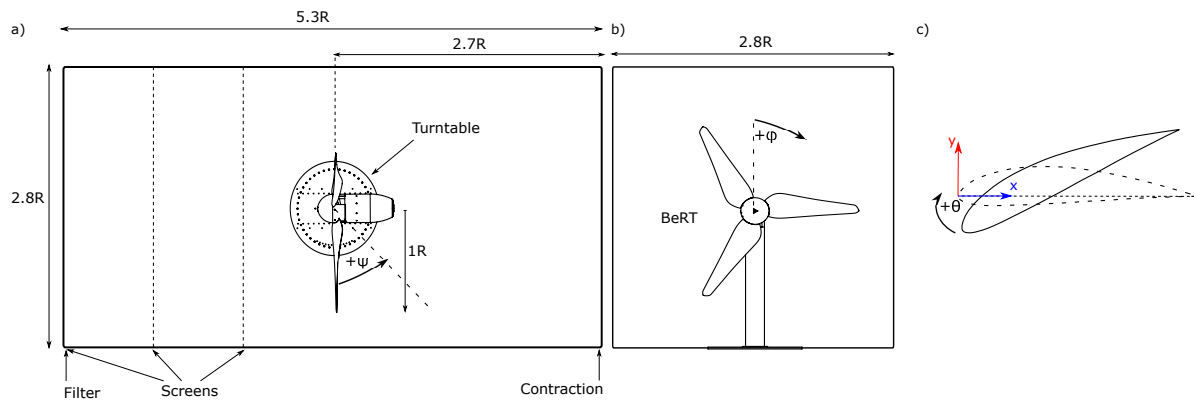
Figure 2. Sketch of BeRT placed in the test section and main angles definition. a) Top view. b) Front view from upstream to downstream. c) Blade arbitrary section and coordinate system.

The turbine, placed in the test section, is shown in Fig. 2 where its main angles definition is presented. One of the blades is equipped with a variety of sensors. The current study presents results from the pressure measurements. A total of 31 pressure taps are located chordwise at 45% of the blade span, 12 taps on the pressure side and 19 taps on the suction side. More details on the sensors and test rig can be found in the previous work of Soto-Valle et al. [27]. The acquisition frequency is set to $10kHz$. Moreover, a Hall effect sensor is positioned in the nacelle to obtain the azimuthal position of the blade during each rotation. Each measurement was recorded and phase-averaged over 100 rotations in groups of $\Delta\phi = 1°$.

Additionally, three simulated datasets are considered in the 3D framework. On the one side, CFD simulations are done by means of unsteady Reynolds-averaged Navier-Stokes computations using the block-structured solver FLOWer, based on the finite volume method. The FLOWer code was originally developed at the German Aerospace Center (DLR) and adapted for wind turbine applications at the University of Stuttgart. Thus, the compressible Navier–Stokes equations are solved, where the temporal discretization uses an implicit dual time-stepping scheme, while the space is discretized with a second-order central JST scheme. Turbulence is modeled by the Menter shear stress transport turbulence model in a fully turbulent state. The mesh of all components is made separately with a fully resolved boundary layer and all grids are overlapped, using the CHIMERA technique. More information can be found in the previous works of Klein et al. [17–19]. Both wind tunnel and far-field simulations are considered in this approach. The cases considered are far-field axial inflow, and wind tunnel axial inflow as well as yaw misalignments $\psi = -15°, -30°$.

On the other side, LLFVW simulations are done using the numerical tool QBlade. The simulations are fed by XFoil. The simulation parameters were kept constant from the 2D approach aforementioned, except by the Re number, which was additionally swept between $Re = (1.0 - 3.5) \times 10^5$ with steps of $\Delta Re = 10^4$, $Re = (1.5 - 3.5) \times 10^5$ with steps of $\Delta Re = 2.5 \times 10^3$ and $Re = (1.5-3.2) \times 10^5$ with steps of $\Delta Re = 2.5 \times 10^4$. Ranges and steps were chosen, after a geometrical estimation of the Re number based on BeRT operational conditions and dividing the blade into three sections $I: 0.15 - 0.4R$, $II: 0.4 - 0.75R$, $III: 0.75 - 1R$. A number of 20 blade panels, azimuthal step of $5°$, initial vortex core size of 10% of the chord station and a turbulent vortex viscosity coefficient of 7.5 are considered. More information can be found in the previous works of Marten et al. [28, 29].

Both CFD and LLFVW simulations were performed under the same operational conditions of BeRT by means of inflow velocity and rotational speed until the blade loads converged and the wake was correctly propagated. Then, five further rotations were computed and phase-averaged accordingly to the azimuthal angle. These codes give the opportunity to test high (CFD) and medium fidelity (LLFVW) simulations, which also are performed at different computational costs. Consequently, a total of six datasets in different conditions are analyzed. Table 2 shows a summary of their conditions. The following section provides the methodology applied to each dataset to perform the comparison.

Table 2. Summary of the datasets considered in this study.

| dataset	approach	type	wind tunnel walls	pitch angle	yaw angle
$BeRT$	experimental	3D	yes	$-10° : 2° : 10°$	$0°, -15°, -30°$
$XFoil$	simulation	2D	no	—	—
2D-wing	experimental	2D	yes	—	—
CFD_{FF}	simulation	3D	no	$0°$	$0°$
CFD_{WT}	simulation	3D	yes	$0°$	$0°, -15°, -30°$
$LLFVW$	simulation	3D	no	$0°$	$0°, -15°, -30°$

3. Methodology

In this section, the data postprocessing methodology is described. The main idea is to compare the measurements from BeRT against 2D and 3D datasets from both experiments and simulations, using either the same airfoil shape or complete wind turbine model. The pressure distribution is used as a common initial point to study the differences due to 3D and blockage effects. Nevertheless, these pressure distributions are obtained in different manners, which are described as follows.

The experimental approaches, BeRT and the 2D-wing, use the information of pressure sensors connected through to the pressure taps located chordwise in the blade or wing, respectively. The pressure values are normalized by the relative dynamic pressure of the wind tunnel [27], which provides the pressure coefficient distribution. Datasets are (1) averaged over time at each AoA, in the case of the 2D-wing; and (2) phase-averaged at each azimuthal station over the complete set of rotations, in the case of BeRT measurements.

XFoil and CFD simulations provide directly the pressure distribution after their execution. In the case of LLFVW, as the output does not provide a pressure distribution of any local station of the blade, both the induced AoA and Re were exported to obtain, based on these values, an XFoil simulation, which provides the local respective set of polar datasets. Consequently, in the blockage analysis, the pressure magnitudes from CFD and BeRT were normalized with respect to their local dynamic pressure, estimated from the maximum pressure magnitude of the pressure side at the respective azimuthal angle station. Figure 3 provides a flowchart summary of the pressure distribution datasets.

Once each of the datasets provides a pressure coefficient distribution, normal and tangential force coefficients are calculated by direct surface pressure integration, Eq. 1. Since there were no pressure taps connected to sensors beyond 90% of BeRT-blade chord, the pressure integration of each dataset was performed until that chord position, in order to quantify the same contributions.
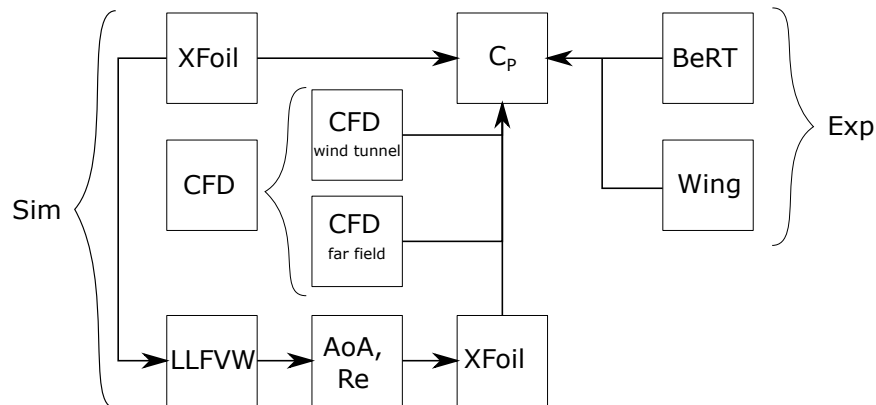
Figure 3. Flow diagram of the sources of each dataset compared in this study.

Additionally, the blade pitch angle of BeRT was used to correlate it to the local AoA [27, 30], based on previous work in the same test rig, Eq. 2.

$$C_n = \oint C_p d(x/c), \ C_t = \oint C_p d(y/c), \tag{1}$$

$$\alpha = 0.7\theta + \alpha_0, \tag{2}$$

where $\alpha_0 = 7.6°$ is the AoA when the blade is at its neutral position, $\theta = 0°$. The quantitative comparison between the different datasets is done with respect to BeRT experiments and by means of the normalized force coefficient difference as is shown in Eqs. 3 and 4.

$$\Delta C_n = 100 \times \frac{C_{n, \ BeRT} - C_{n, \ to \ compare}}{C_{n, \ BeRT}}, \tag{3}$$

$$\Delta C_t = 100 \times \frac{C_{t, \ BeRT} - C_{t, \ to \ compare}}{C_{t, \ BeRT}}. \tag{4}$$

4. Results
Results are presented as follows. First, a comparison between the calculated force coefficients on the rotating BeRT blade and the 2D approaches is presented (Sect. 4.1). The numerical (XFoil) and experimental (2D-wing) results are presented in order to highlight the 3D effects in the rotating frame. Only axial inflow conditions are taken into account for this comparison. Secondly, Sect. 4.2 shows a comparison between force coefficients of the rotating BeRT blade and 3D computations with and without considering the wind tunnel walls. In this section, cases with yaw misalignment are also examined.

4.1. 3D effects
In this section 2D approaches are compared against the rotating blade of BeRT. Figure 4 shows the normal and tangential force coefficients derived from the full set of pressure distributions. The normal force coefficients, Fig. 4a) behave linearly for all the approaches until an angle of attack $\alpha \approx 10°$. Moreover, the small magnitude differences are within the range of the uncertainty of the blade data. Beyond that, both XFoil and the 2D-wing present a convex shape with smaller magnitude than the rotating blade due to the airfoil stall. The difference is explained by the rotational augmentation. Indeed, the rotating blade exhibits an evident delay in the stall condition. Here the relative normal force coefficient differences with respect to BeRT

are between $3-12\%$ and $7-18\%$ for XFoil and 2D-wing, respectively. It is noticed a lower force magnitude of the 2D-wing compared to the simulation, which is attributed to the formation of a stall cell [31, 32].
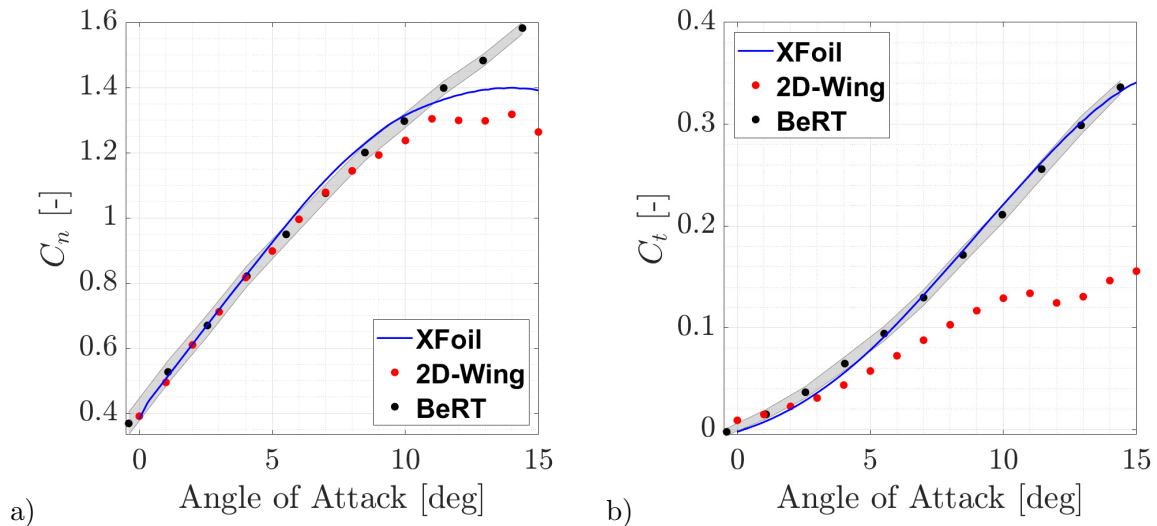
Figure 4. Force coefficients over the angle of attack of BeRT, XFoil and 2D-Wing. BeRT is under axial inflow ($\psi = 0°$). a) Normal force coefficient. b) Tangential force coefficient.

In the case of the tangential force, Fig. 4b), the rotating blade and XFoil simulation follow the same trend all over the AoA range described here. In fact, the influence on the tangential force due to rotation is also known as centrifugal pumping and is studied regarding drag coefficient. Because of this, it is often considered to be small and many models do not even propose a correction [3], in agreement with the current findings. In the case of the 2D-wing, two possible explanations are hypothesized for the lower tangential force magnitude. On the one side, it is likely that the roughness, produced by the flap hinge, contributes to a larger drag. On the other side, a stall cell formation is conceivable; thus, the tangential force coefficient decrement becomes more evident by the 3D effects produced by this phenomenon. In addition, it is known that XFoil simulations produce lower drag, which increases the difference between the 2D approaches.

Overall, the rotational augmentation is evident due to the presence of stall delay in the rotating blade results, despite the large blockage. Therefore, to get a better insight into the blockage effects over the pressure distribution and their respective derived forces, the following section addresses such a concept.

4.2. Blockage effects
Several 3D approaches are compared against the rotating blade of BeRT. Each approach is presented by its phase-averaged result and a light-colored area, which corresponds to its standard deviation. Both statistical analyses are done with respect to the azimuthal angle.
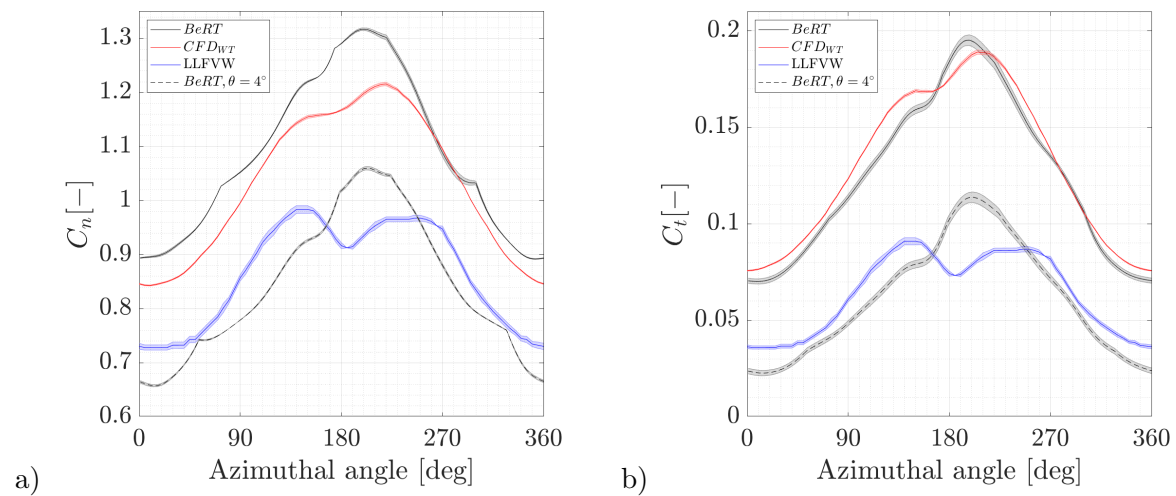
Figure 5 shows the force coefficients over azimuthal angles under axial inflow. It can be noticed that all the curves show a noticeable feature at the azimuthal angle $180°$, a product of the tower shadow effect. Additionally, far-field and wind tunnel approaches have similar force coefficient magnitudes, whereas the largest values are for the wind tunnel approaches as a consequence of the blockage. The latter implies an increase in efficiency and mass flow rate because the flow is not expanding either upstream or downstream of the rotor as it would do in unconfined conditions, leading to an overall increase in local forces.
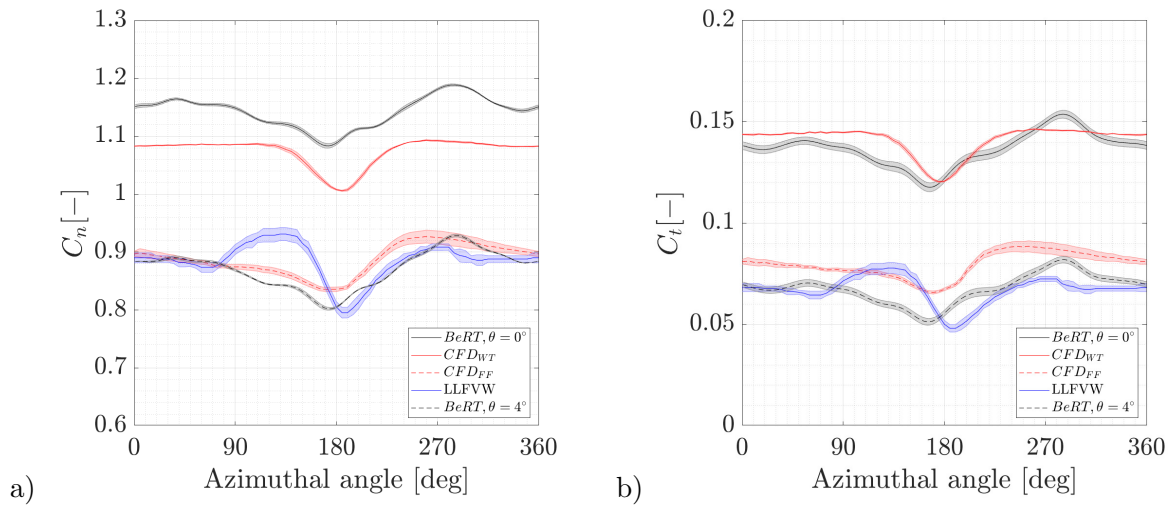
Figure 5. Force coefficients over azimuthal angle of BeRT experiments, CFD (FF:far field, WT: wind tunnel)and LLFVW simulations under axial inflow. a) Normal force coefficient. b) Tangential force coefficient.

A small relative difference for both force coefficients from the CFD simulation is noticed, when the wind tunnel is considered. These differences are up to 9% and −12% for normal and tangential force coefficients, respectively. These variations change along with the azimuthal angle and are deemed due to the differences in the inflow, where BeRT test rig presents some heterogeneity compared to the CFD simulation [19,27]. Despite the small difference, CFD results are qualitatively closer to experiments, while LLFVW has an unexpected increase between azimuthal angles $90° − 180°$.

When BeRT experiments are compared to far-field approaches, both normal and tangential force coefficients present a qualitative offset from the wind tunnel approaches. In relative terms, the differences go to a maximum of $\Delta C_n \approx 28\%$ and $\Delta C_t \approx 62\%$. It is remarkable that, when BeRT-blades are pitched by 4° (Figure 5, black dashed line), experimental results get closer to the far-field simulations reducing discrepancies between both the two force coefficients. Thus, pitching the blades counteracts the blockage effect locally. Figure 6 depicts the normal and tangential force coefficients over azimuthal angles under a yaw misalignment of −15°. Regarding the wind tunnel applications, both force coefficients continue describing the same trends with lower magnitudes in the case of CFD simulations. In both cases, there is a prediction of the tower shade but only as a small shift in the trends of the curves. The wind tunnel approaches still present larger magnitudes than LLFVW. In both force coefficients, the LLFVW simulation shows a noticeable location of the tower. After pitching BeRT-blades, the experiments still match well with the simulations that neglects the wind tunnel walls even though the high yaw misalignment. It is also perceived some sharp locations in the experiments from BeRT. These are caused by the local normalization, which changes depending on the pressure taps that provides the maximum pressure magnitude in the pressure side of the blade [27].

Figure 6. Force coefficients over azimuthal angle of BeRT experiments, CFD (WT: wind tunnel) and LLFVW simulations under a misalignment of $15°$. a) Normal force coefficient. b) Tangential force coefficient.

Figure 7 shows the normal and tangential force coefficients over azimuthal angle under a yaw misalignment of $-30°$. Between the wind tunnel approaches trends are conserved from the previous case with a steeper curve. At this severe yaw misalignment, all the curves become closer, which might be due to the reduction in the blockage after the yawing. Furthermore, the closest blade pitch angle that counteracts the blockage is now $\theta = 2°$; however, the tower shade effect is now completely covered by the crossflow. Conversely, the LLFVW simulation does not show an increment closer to the tower due to the high AoA at this azimuthal station.
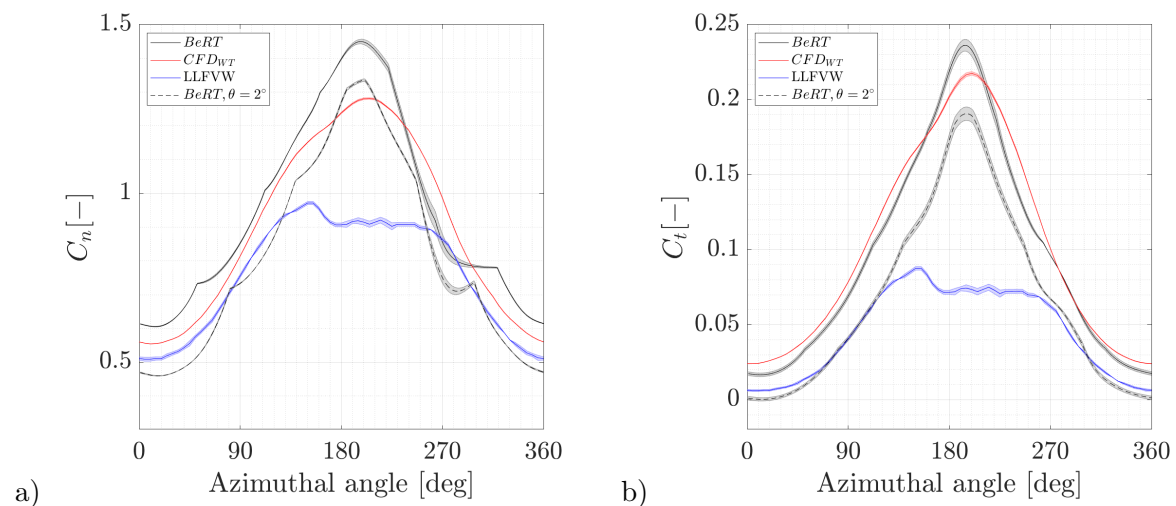
Figure 7. Force coefficients over azimuthal angle of BeRT experiments, CFD (WT: wind tunnel) and LLFVW simulations under a misalignment of $30°$. a) Normal force coefficient. b) Tangential force coefficient.

5. Conclusions

An extensive database of the Berlin Research Turbine (BeRT) rotor blade in terms of force distributions at the local span at $45\%R$ of the blade is presented. The experiments are compared to several datasets from experiments and simulations with 2D and 3D approaches. The most important remarks concerning the local rotational effects as well as the blockage consequences are:

- The presence of rotational augmentation is evident and exhibited the expected relative effects despite the wind tunnel blockage. The maximum local normal force coefficient of the rotating blade is 12% more than in simulations and 18% more than in the 2D-wing, delaying the stall at least $4°$.

- The local tangential force coefficient presents the same trend and magnitudes in the rotating blade and 2D simulations.

- The wind tunnel causes a maximum relative increment of 28% in the local normal and 62% in the local tangential force coefficients with respect to the wind turbine experiments in axial inflow.

- A high yaw misalignment, $\psi = -15°$, conserves trends relative differences between wind tunnel and far-field simulations.

- A severe yaw misalignment, $\psi = -30°$, reduces the local force coefficient differences between wind tunnel and far-field simulations.

- Pitching the blade in experiments counteracted the impact of the blockage locally, obtaining similar values in the local forces when the far-field simulations maintain the blade pitch angle equal to zero.

Further studies will include the global influence of the blockage on the blade by means of the study of the blade root bending moment in a larger simulation dataset.

Acknowledgments

References

[1] Schreck S 2008 IEA wind annex xx: Hawt aerodynamics and models from wind tunnel measurements; final report Tech. rep. National Renewable Energy Lab.(NREL), Golden, CO (United States)

[2] Hand M, Simms D, Fingersh L, Jager D, Cotrell J, Schreck S and Larwood S 2001 Unsteady aerodynamics experiment phase vi: wind tunnel test configurations and available data campaigns Tech. rep. National Renewable Energy Lab., Golden, CO.(US)

[3] Guntur S and Sørensen N 2013 *A detailed study of the rotational augmentation and dynamic stall phenomena for wind turbines* Ph.D. thesis Ph. D. thesis, Technical Univ. of Denmark, Lyngby, Denmark

[4] Schepers J, Boorsma K, Cho T, Gomez-Iradi S, Schaffarczyk P, Jeromin A, Shen W Z, Lutz T, Meister K, Stoevesandt B *et al.* 2012 Analysis of mexico wind tunnel measurements: Final report of iea task 29, mexnext (phase 1) Tech. Rep. ECN-E–12-004 Energy research Centre of the Netherlands (ECN)

[5] Sant T, van Kuik G and Van Bussel G 2009 *Wind Energy: An International Journal for Progress and Applications in Wind Power Conversion Technology* **12** 1–32

[6] Sant T, van Kuik G and Van Bussel G 2006 *Wind Energy: An International Journal for Progress and Applications in Wind Power Conversion Technology* **9** 549–577

[7] Bechmann A, Sørensen N N and Zahle F 2011 *Wind Energy* **14** 677–689

[8] Zhang Y, van Zuijlen A and van Bussel G 2017 *Journal of Wind Engineering and Industrial Aerodynamics* **168** 152–163

[9] Schümann H, Pierella F and Sætran L 2013 *Energy Procedia* **35** 285–296

[10] Hassanzadeh A, Naughton J W, LoTufo J and Hangan H 2020 *Journal of Physics: Conference Series* vol 1452 p 012059

[11] Campanardi G, Grassi D, Zanotti A, Nanos E M, Campagnolo F, Croce A and Bottasso C L 2017 *Journal of Physics: Conference Series* **882** 012003 URL https://doi.org/10.1088/1742-6596/882/1/012003

[12] Schottler J, Mühle F, Bartl J, Peinke J, Adaramola M S, Sætran L and Hölling M 2017 *J. Phys. Conf. Ser* vol 854 p 012032

[13] Bayati I, Bernini L, Zanotti A, Belloli M and Zasso A 2018 *Journal of Physics: Conference Series* **1037** 052024 URL https://doi.org/10.1088/1742-6596/1037/5/052024

[14] Pechlivanoglou G, Fischer J, Eisele O, Vey S, Nayeri C and Paschereit C 2015 *12th German Wind Energy Conf. (DEWEK), Bremen, Germany*

[15] Vey S, Marten D, Pechlivanoglou G, Nayeri C and Paschereit C O 2015 *33rd AIAA Applied Aerodynamics Conference* p 3392

[16] Huang X, Vey S, Meinke M H, Schroeder W, Pechlivanoglou G, Nayeri C and Paschereit C O 2015 *45th AIAA Fluid Dynamics Conference* p 2310

[17] Fischer A, Flamm A, Jost E, Lutz T and Krämer E 2018 *New Results in Numerical and Experimental Fluid Mechanics XI* (Springer) pp 717–727

[18] Klein A, Zabel S, Lutz T and Krämer E 2018 *High Performance Computing in Science and Engineering'17* (Springer) pp 339–353

[19] Klein A C, Bartholomay S, Marten D, Lutz T, Pechlivanoglou G, Nayeri C N, Paschereit C O and Krämer E 2018 *Wind Energy Science* **3** 439–60

[20] Soto-Valle R, Alber J, Manolesos M, Nayeri C N and Paschereit C O 2020 *Journal of Physics: Conference Series* **1618** 032045

[21] Marten D, Lennie M, Pechlivanoglou G, Nayeri C N and Paschereit C O 2016 *Journal of Engineering for Gas Turbines and Power* **138** 072601

[22] Alber J, Soto-Valle R, Manolesos M, Bartholomay S, Nayeri C N, Schönlau M, Menzel C, Paschereit C O, Twele J and Fortmann J 2020 *Wind Energy Science* **5** 1645–1662 URL https://wes.copernicus.org/articles/5/1645/2020/

[23] Soto-Valle R, Bartholomay S, Manolesos M, Nayeri C N and Paschereit C O 2021 Airfoil shaped vortex generators applied on a research wind turbine accepted for 2021 AIAA SciTech Forum

[24] Bartholomay S, Michos G, Perez-Becker S, Pechlivanoglou G, Nayeri C, Nikolaouk G and Paschereit C O 2018 *Proc. Wind Energy Symposium, American Institute of Aeronautics and Astronautics, Kissimee, Florida, USA*

[25] Bartholomay S, Wester T T B, Perez-Becker S, Konze S, Menzel C, Hölling M, Spickenheuer A, Peinke J, Nayeri C N, Paschereit C O and Oberleithner K 2021 *Wind Energy Science* **6** 221–245 URL https://wes.copernicus.org/articles/6/221/2021/

[26] Wei N J, Kissing J, Wester T T, Wegt S, Schiffmann K, Jakirlic S, Hölling M, Peinke J and Tropea C 2019 *Journal of Fluid Mechanics* **876** 237–263

[27] Soto-Valle R, Bartholomay S, Alber J, Manolesos M, Nayeri C N and Paschereit C O 2020 *Wind Energy Science* **5** 1771–1792 URL https://wes.copernicus.org/articles/5/1771/2020/

[28] Marten D, Bartholomay S, Pechlivanoglou G, Nayeri C, Paschereit C O, Fischer A and Lutz T 2018 *2018 Wind Energy Symposium* p 1246

[29] Marten D, Paschereit C O, Huang X, Meinke M, Schroeder W, Mueller J and Oberleithner K 2020 *AIAA Journal* 1–14

[30] Soto-Valle R, Noci S, Papi F, Bartholomay S, Nayeri C N, Paschereit C O and Bianchini A 2021 *E3S Web of Conferences* vol 312 p 08003

[31] Manolesos M, Papadakis G and Voutsinas S G 2014 *Wind Energy* **17** 939–955

[32] Olsen A S, Sørensen N N, Bak C, Gaunaa M, Mikkelsen R, Fischer A, Beckerlee J and Ildvedsen S 2020 *Journal of Physics: Conference Series* **1618** 032040 URL https://doi.org/10.1088/1742-6596/1618/3/032040